Assessment of the Performance of a Dual-Frequency Surface Reference Technique

R. Meneghini, *Senior Member, IEEE*, L. Liao, S. Tanelli, and S. L. Durden, *Senior Member, IEEE*

Abstract— The high correlation of the rain-free surface cross sections at two frequencies implies that the estimate of differential path integrated attenuation (PIA) caused by precipitation along the radar beam can be obtained to a higher degree of accuracy than the path-attenuation at either frequency. We explore this finding first analytically and then by examining data from the JPL dual-frequency airborne radar using measurements from the TC4 experiment obtained during July-August 2007. Despite this improvement in the accuracy of the differential path attenuation, solving the constrained dual-wavelength radar equations for parameters of the particle size distribution requires not only this quantity but the single-wavelength path attenuation as well. We investigate a simple method of estimating the single-frequency path attenuation from the differential attenuation and compare this with the estimate derived directly from the surface return.

***Index Terms*—attenuation, precipitation, radar, surface scattering**

I. Introduction

The surface reference technique is based on the idea that a decrease in the surface return power in the presence of precipitation relative to a rain-free reference value provides an estimate of the two-way path attenuation caused by precipitation along the radar beam. The method has been shown to be useful particularly at higher rain rates and under certain combinations of incidence angle and surface type (land/ocean) where the path attenuations are much larger than the inherent fluctuations in the surface scattering cross section. The method has been applied to both airborne and spaceborne radar data [1-11].

The Global Precipitation Measurement (GPM) satellite is scheduled to be launched in 2013 where the set of instruments on board will include the first spaceborne dual-frequency precipitation radar (DPR), built by the Japan Aerospace Exploration Agency (JAXA). The frequencies of operation are Ku-band (13.6 GHz) and Ka-band (35.5 GHz). Of interest here is the fact that matched-beam, dual-frequency radar data will be acquired over a swath of approximately 120 km, consisting of 25 fields of view, including nadir and extending, to either side of nadir, out to approximately 9^0.

With dual-frequency radar comes the potential of estimating parameters of the particle size distribution (PSD) for rain and snow along the radar beam [12-17]. In the backward recursion formulation of the equations, the differential path-integrated attenuation and the path-attenuation at one of the frequencies are required. Denoting the path integrated attenuation (PIA) by A, in dB, then the differential path attenuation, δA, is defined by $\delta A = A(Ka) - A(Ku)$.

We show in section 2 that the error variance of the differential attenuation derived from the surface reference method is smaller than the surface-reference derived attenuation at either frequency if the correlation in the rain-free surface cross sections is high. Experimental data indicates that this is the case at most incidence angles from 0 to 20 degrees over both ocean and land.

It is also instructive to consider this relationship graphically in the $(\sigma^0(Ku), \sigma^0(Ka))$ plane where the distance between the measured data point, in rain, to the regression line of the rain-free data is proportional to $A(Ka) - \beta A(Ku)$, where β, usually close to one, is the slope of the regression line. At $\beta = 1$, this distance becomes directly proportional to the differential attenuation, δA, implying that this estimate is invariant to changes in the reference data along the regression line.

A third way to show this improvement is by comparing error estimates of the single- and dual-wavelength retrievals of attenuation using airborne dual-wavelength radar data. In this third way we look at a more realistic scenario which resembles the implementation in the operational SRT algorithm. In this approach, each of the SRT estimates for Ku, Ka and the differential attenuation is obtained as a weighted sum of various spatial reference estimates. In the case of the differential attenuation estimate, the different spatial estimates are shown to be in good agreement. In contrast, the single-wavelength SRT estimates often show that the various reference data sets yield significant differences in the PIA.

Even though the SRT should provide in many cases a more accurate estimate of differential attenuation than the attenuation itself, as noted above, many approaches to estimating parameters of the size distribution from the dual-

Manuscript received March 31, 2011

R. Meneghini is with NASA Goddard Space Flight Center, Greenbelt, MD 20771, U.S.A. (phone: 301-614-5652; fax: 301-614-5492; e-mail: robert.meneghini-1@ nasa.gov).

L. Liao is with Goddard Earth Science Technology/UMBC, Code 613.1, NASA/GSFC, Greenbelt, MD (email: liang.liao-1@nasa.gov)

S. Tanelli is with Jet Propulsion Laboratory, California Institute of Technology, Pasadena, CA, 91109 (e-mail: simone.tanelli@nasa.gov).

S.L. Durden is with Jet Propulsion Laboratory, California Institute of Technology Pasadena, CA, 91109 (e-mail: steven.l.durden@nasa.gov).

frequency radar data require the attenuation at a single frequency as well as the differential. Stated differently, not only is δA required but A(Ka) or A(Ku). If A(Ka) is estimated from δA, an additional error is incurred that depends on the particle size distributions of the precipitation along the beam; on the other hand, if A(Ka) is estimated by the single-wavelength SRT, the error is primarily determined by the variations in the surface cross section. We show comparisons of the two approaches and the conditions under which one might be preferable to the other. It is worth noting that although the surface return at two frequencies offers insight into the non-uniform beamfilling problem [18, 19], this topic is beyond the scope of the paper.

II. BASIC APPROACH AND GENERAL CONSIDERATIONS

Estimates for the SRT-derived PIA can be written either as functions of the radar return powers from the surface or the normalized radar cross sections (NRCS) of the surface. Here, we will use exclusively the latter quantity. The rain-free reference for the NRCS is generally taken as an average of the rain-free NRCS values outside the raining area or at earlier or later times at the raining area when rain is absent. We denote this rain-free NRCS average by $<\sigma^0_{NR}>$ while the apparent or measured NRCS over the radar beam of interest in the presence of precipitation is denoted by σ^0_m. An estimate of δA is obtained from the following equation:

$$\delta A(f_{1,}f_2) = [<\sigma^0_{NR}(f_1)> - \sigma^0_m(f_1)] - [<\sigma^0_{NR}(f_2)> - \sigma^0_m(f_2)] \quad (1)$$

where all quantities are expressed in dB. We assume that $f_1>f_2$ so that f_1 is associated with the Ka-band and f_2 with the Ku-band frequency. Since the objective here is to obtain an approximate expression for the variance, we neglect errors caused by a finite number of samples and write

$$\sigma^0_m(f) = \sigma^0(f) - A(f) \quad (2)$$

where σ^0 is the unattenuated NRCS at the raining area of interest and A is the two-way path-integrated attenuation from the radar to the surface. This is related to the specific attenuation, k, in dB/km, by

$$A(f) = 2\int_0^{r_s} k(f,s)ds \quad (3)$$

It is worth noting that k is the sum of attenuation contributions from precipitation, cloud and atmospheric gases. What fractions of these constituents get included in the path attenuation estimate depend on the detection threshold of the radar and the amounts of cloud water, water vapor and precipitation present in the areas from which the reference data are taken. The integral in (3) is taken along the radar beam from the radar (r=0) to the surface ($r=r_s$). Substituting (2) into (1) gives

$$\delta A(f_{1,}f_2) = \delta A_T(f_{1,}f_2) + [<\sigma^0_{NR}(f_1)> - \sigma^0(f_1)] - [<\sigma^0_{NR}(f_2)> - \sigma^0(f_2)] \quad (4)$$

where δA_T denotes the true value of the differential attenuation. In taking the variance of (4) we assume that the variance and covariance terms involving the rain-free sample mean data can be neglected. With this assumption, the variance can be approximated by:

$$\mathrm{var}(\delta A(f_{1,}f_2)) \approx \mathrm{var}(\sigma^0(f_1)) + \mathrm{var}(\sigma^0(f_2)) - 2\rho[\mathrm{var}(\sigma^0(f_1))\,\mathrm{var}(\sigma^0(f_2))]^{0.5} \quad (5)$$

Where ρ is the correlation coefficient associated with the unattenuated NRCS at the raining area. Eq. (5) reduces to 0 when $\rho=1$ and $\mathrm{var}(\sigma^0(f_1))=\mathrm{var}(\sigma^0(f_2))$. It should be emphasized that Eq. (5) is an approximation where fluctuations caused by sampling errors and variations in the sample means of the reference data have been neglected. Using the same approximations for the single-wavelength surface reference estimate, we obtain $\mathrm{var}(A(f)) = \mathrm{var}(\sigma^0(f))$ so that an equation analogous to (5) can be written for the single-frequency SRT:

$$\mathrm{var}(A(f_{i,})) \approx \mathrm{var}(\sigma^0(f_i)); i = 1,2 \quad (6)$$

Assuming that the variances of σ^0 are comparable at the two frequencies, then these results suggest that the estimate of δA should have a smaller variance than A when the correlation coefficient of the rain-free NRCS is greater than about 0.5.

A way of visualizing the relationship between the single- and dual-frequency implementations of the SRT is shown in Fig. 1. The rain-free reference (labeled R) represents the data point $(<\sigma^0_{NR}(f_1)>, <\sigma^0_{NR}(f_2)>)$ in the $\sigma^0(f_1)$- $\sigma^0(f_2)$ plane. Likewise, the apparent surface cross sections measured in the precipitating medium, $(\sigma^0_m(f_1), \sigma^0_m(f_2))$, is labeled M. The attenuation estimate $A(f_1)$ is then equal to the projection onto the $\sigma^0(f_1)$ axis of the line segment between R and M; similarly, $A(f_2)$ is the projection of this line onto the $\sigma^0(f_2)$ axis. Also shown in the figure is the regression line of slope β, where $\theta=\mathrm{Tan}^{-1}\beta$. The regression line is assumed to be determined in the usual way by minimizing the rms error between the line and the rain-free reference data points. Because of this, the point R will fall on the regression line since this point represents the sample mean of the rain-free reference data. The distance D shown on the figure is defined as the perpendicular distance from M to the regression line. From the figure, we have the following relationships

$$D = [A^2(f_1) + A^2(f_2)]^{0.5} \sin\gamma$$

$$\sin\gamma = \sin(\pi/2 - \theta - \varsigma) = \cos(\theta + \varsigma)$$
$$= [A(f_1) - \beta A(f_2)]/[(1+\beta^2)(A^2(f_1) + A^2(f_2))]^{0.5} \quad (7)$$

$$D = [A(f_1) - \beta A(f_2)]/(1+\beta^2)^{0.5}$$

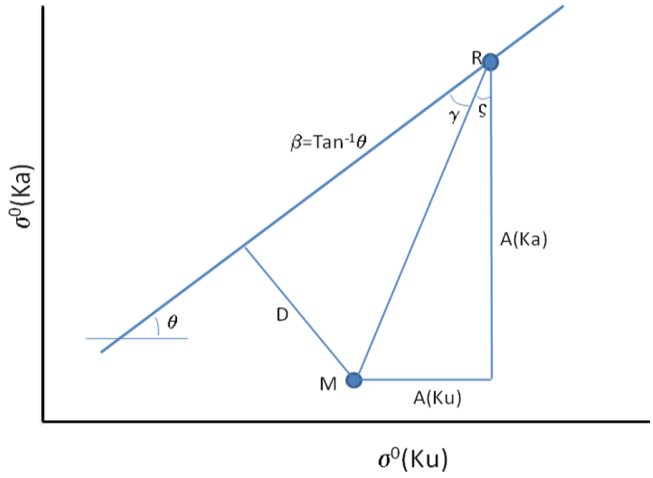

Fig.1. Schematic diagram showing how A(Ka) and A(Ku) are computed from the measured data in rain (M) relative to the reference or rain-free data (R). As noted in the text, the perpendicular distance, D, of M to the regression line is proportional to A(Ka)-βA(Ku) which is equal to the differential attenuation when the slope of the regression line, β, is one.

As the slope of the regression line is often close to 1, the distance D is approximately proportional to the differential attenuation. This implies that a displacement in R along the regression line has no effect on δA since δA depends only on the distance of M to the regression line and not on the location of the reference data point on the regression line. In contrast, it can be seen from the figure that a displacement in R along the regression line changes both $A(f_1)$ and $A(f_2)$.

III. ANALYSIS OF AIRBORNE DUAL-FREQUENCY RADAR DATA

The JPL Airborne Precipitation Radar (APR 2) is a dual-frequency Doppler system operating at 13.4 GHz (Ku-band) and 35.6 GHz (Ka-band) with approximately matched beams and with a cross-track scan ranging from $\pm 25^0$ of nadir [20]. Because of the similarities between the APR 2 and DPR with respect to the frequencies, scanning geometry and matched beams, the data provide insight into the expected performance of the DPR. The APR 2 data analyzed here were measured over the July-August period of 2007 during the NASA Tropical Composition, Cloud and Climate Coupling (TC4) experiment, based in Costa Rica with flights primarily over the tropical region of the Eastern Pacific.

A segment of the APR 2 data is presented in Fig. 2 where the measured (without attenuation correction) radar reflectivity factors at near-nadir incidence, $dBZ_m(Ku)$ and $dBZ_m(Ka)$, are shown in the top two panels. (A short period during which the aircraft was banking occurs near sequence number 5100). Two sets of PIA values are shown in the center panel where the blue lines represent the Ku-band estimates and the red lines the Ka-band estimates. Descriptions of the various PIA estimates are deferred until later in this section. The data in the bottom two panels represent the σ^0 values at Ku and Ka-band as functions of the incidence angle (ordinate). Note that the abscissa represents the sequence or observation number where an observation consists of radar data acquired over a period of 1.8 seconds.

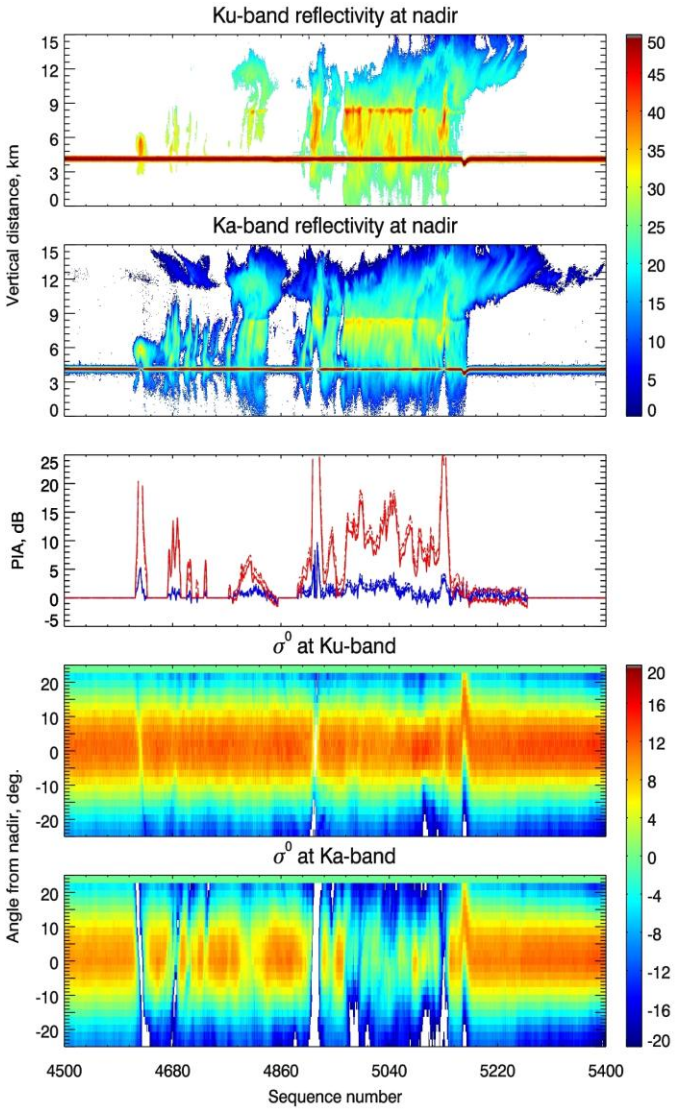

Fig.2. APR 2 data over a flight segment of approximately 30 min. Top: Measured radar reflectivity factors at Ku-band and Ka-band at near-nadir incidence; Center: PIA estimates at Ka-band (red) and Ku-band (blue) at near-nadir incidence; Bottom: σ^0 over the full swath (ordinate) at Ku- and Ka-band.

Examples of scatter plots of σ^0(Ka) versus σ^0(Ku) at several incidence angles under rain-free conditions are shown in Fig. 3. Additional statistics are given in Table 1. Of primary interest are the correlation coefficients that increase from a value of about 0.6 at near-nadir incidence to values of 0.98-0.99 for angles at 11^0 and higher. These results suggest that the SRT-based differential attenuation estimates should be substantially better than the single-wavelength results for off-nadir incidence angles but with more modest improvements at near-nadir angles. (It should be noted that an analysis over a larger data set suggests that correlations at near-nadir incidence are higher (0.7-0.8) than those reported here for the TC4 data set.)

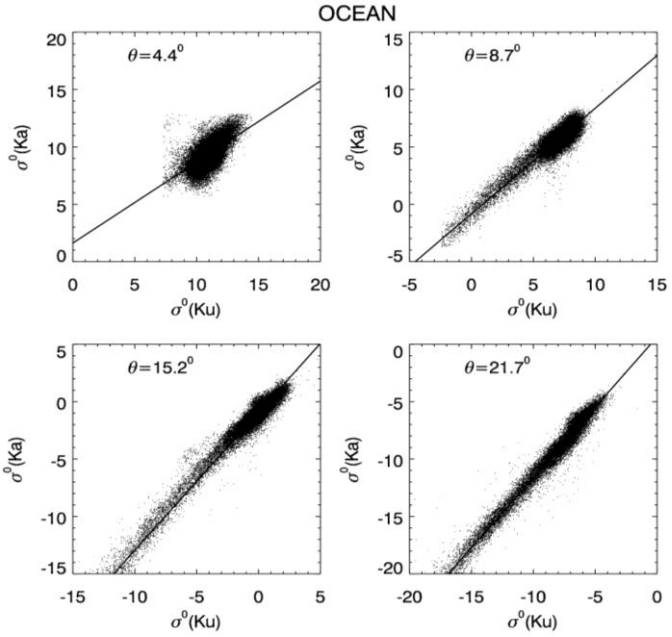

Fig.3. Scatter plots of σ^0(Ku) versus σ^0(Ka) and the linear regression lines at four incidence angles under rain-free conditions for an ocean background.

In the absence of an independent measurement of path attenuation, it is difficult to verify the accuracy of the estimates. Nevertheless, the consistency and stability of the attenuation estimates can be assessed by examining the PIA results from different types of reference data. In the simplest implementation of the SRT, running means and mean squares of the rain-free data are updated (over a fixed number of prior fields of view) at each incidence angle until rain is encountered. When rain is detected at a particular incidence angle, the rain-free average at that angle is used for the reference data so that the PIA is estimated as the difference between the rain-free NCRS average and the apparent NCRS measured at the rainy field of view. An indication of the relative error of the estimate is found by comparing the magnitude of the estimated PIA with the standard deviation of the rain-free data used to form the average. A simple variant of this forward along-track processing is obtained by processing the data backwards so that rain-free data from the opposite end of the storm cells are used as reference. Thus, for ocean background cases where the spatial changes in the wind speed are large, correspondingly large changes may occur in the reference data, and therefore in the PIA estimate, particularly at those incidence angles that are sensitive to wind speed.

A second type of reference data can be formed by recognizing that under no-rain conditions, the cross-track variation in σ^0 over ocean is approximately quadratic [6, 7]. (As noted in [7], deviations of the TRMM PR data from a quadratic fit require some modification of the fitting function. For the processing presented here, a piece-wise quadratic fit is used, one fit for the data in the inner swath (-10^0 to 10^0) and another for data in the two portions of the outer swath (10^0 to 25^0 and -10^0 to -25^0)). In performing the quadratic fits, the running means of the rain-free data at each incidence angle are used as the input data with a weighting inversely proportional to the variance of the rain-free data that are used to compute the average. As with the along-track procedure, this cross-track reference can be run backwards as well as forwards. These four types of reference data (forward/backward along track and forward/backward cross track) yield four PIA estimates. Moreover, the processing can be applied separately to the single-frequency data (Ku and Ka-band) as well as to the differential data. Finally, it is worth mentioning that for satellite data, a fifth type of reference data set is used. Because the surface cross sections at or near the rainy area can be measured under rain-free conditions both before and after the rain event, this temporal reference data set can be formed. However, for airborne field campaigns, these reference data are seldom available.

IV. ERROR ESTIMATES AND RESULTS

Figures 4-6 show comparisons of various pairs of PIA estimates corresponding to the 4 types of reference data described in the previous section. The PIA data were obtained from processing the rain data at a fixed incidence angle, with respect to nadir, of approximately 8.7^0. Path attenuation results for Ku-band and Ka-band are shown in Figs. 4 and 5, respectively. The differential attenuation results are given in Fig. 6. Comparisons between the results in Figs. 4 and 5 indicate that the absolute magnitude of the scatter at Ku- and Ka-band is approximately the same. However, the relative error is much smaller at Ka-band because the attenuations are on the order of a factor of 5 times larger. The variations in the differential PIA estimates shown in Fig. 6 are smaller than the Ku and Ka-band single wavelength results both in an absolute and relative sense. This result suggests that the differential attenuation for the DPR has the potential to be significantly more accurate than the Ku- or Ka-band attenuations derived separately from the SRT.

Results for angles higher than about 4^0 show similar trends; on the other hand, for the angles close to nadir, the differential attenuation results degrade and the single attenuation results improve. This is consistent with the expectation that the relative quality of the results (single versus dual-wavelength PIA) depend on the correlation between the rain-free NRCS and the variance of the NRCS (Eq. 5).

To get a more quantitative assessment of the behavior of the estimates, we consider the following error variance E^2:

$$E^2 = \sum_j w_j (PIA_{eff} - PIA_j)^2 / \sum_j w_j \quad (8)$$

where

$$PIA_{eff} = \sum_j w_j PIA_j / \sum_j w_j \quad (9)$$

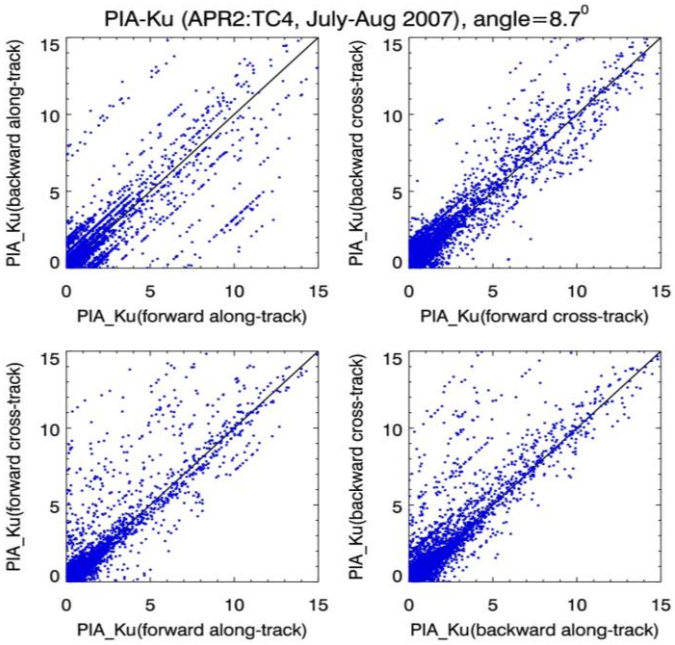

Fig.4. Scatter plots of PIA estimates at Ku-band at an incidence angle of 8.7^0.

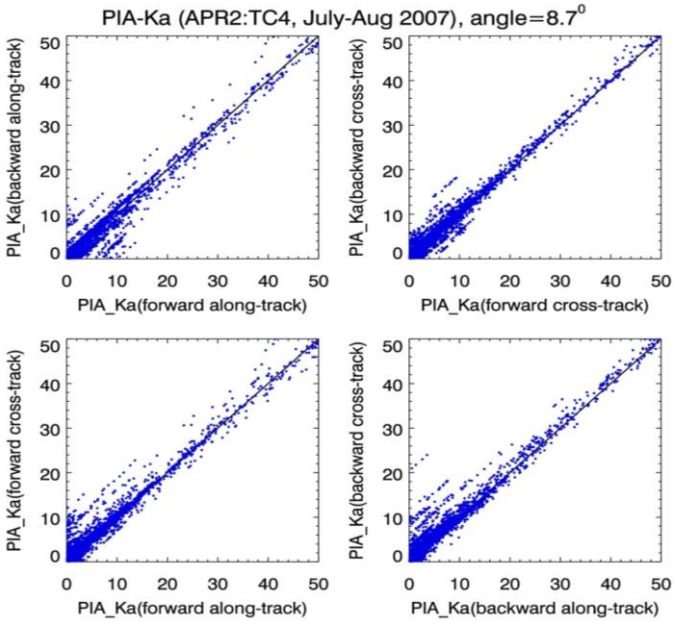

Fig.5. Scatter plots of PIA estimates at Ka-band at an incidence angle of 8.7^0.

$$w_j = 1/\mathrm{var}(PIA_j) \quad (10)$$

where j ranges over the four PIA estimates described above. In these equations, PIA can represent either A(Ku), A(Ka) or δA. The error above, based on a suggestion by Dr. Toshio Iguchi [personal communication], characterizes the mean square deviation of the individual PIA estimates from the estimate of the effective PIA. When the weights of the various estimators are comparable, E is basically the rms deviation from the mean of the four estimates.

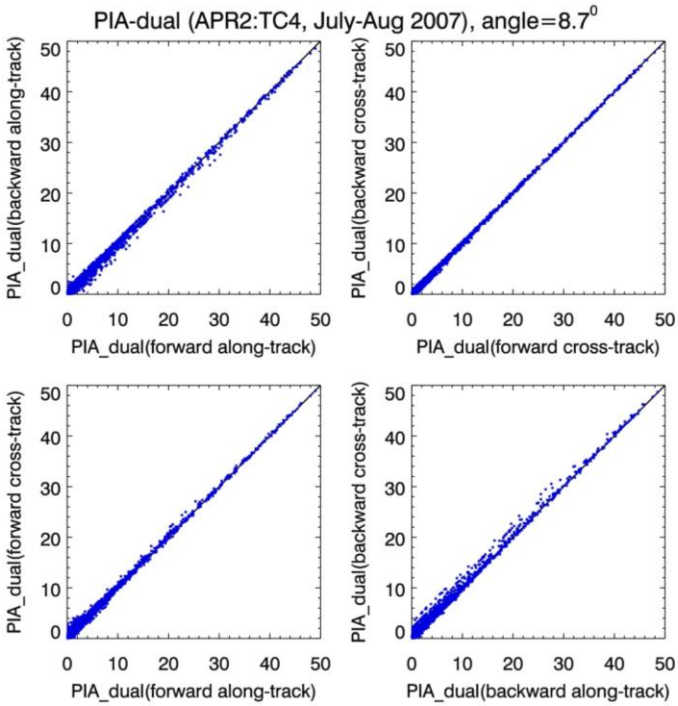

Fig.6. Scatter plots of the differential PIA estimates at an incidence angle of 8.7^0.

Plots of E_{Ku}, E_{Ka}, and E_{dual} for an incidence angle of 8.7^0 over ocean are shown in Fig. 7. Averages of E over the data from each incidence angle are shown in Table 2 for incidence angles from about 2^0 to 22^0 with respect to nadir. Notice that the largest improvements in the use of the dual-frequency SRT relative to the single-frequency occur at higher incidence angles. For example, at an incidence angle of 19.6^0, the average difference in error between the dual-frequency estimate of path attenuation and the single frequency estimate is approximately (2.1-0.44) or 1.7 dB in the case of the Ka-band estimate and (1.65-0.44) or 1.2 dB for the Ku-band estimate. It also should be noted that the error in dual-frequency estimate attains its minimum value at angles in the region from about 8^0 to 11^0 whereas the single-frequency estimates attain a minimum error around 4^0. These results are consistent with the approximate results for the variance of δA and A in (5) and (6), respectively, along with the results in Table 1. In particular, although the variances in σ^0 at both frequencies decrease with angle down to about 4^0, the correlation coefficient also decreases which implies that the variance of δA should attain a minimum before the variances

in the single-frequency path attenuation, which are directly proportional to the variance of σ^0. As shown in the results of Table 2, the least amount of improvement (over ocean) tends to be at near-nadir angles, out to about 4^0, where the dual-frequency estimate offers only a modest improvement in accuracy.

As noted in the introduction, the use of dual-frequency radar data to estimate parameters of the particle size distribution using a backward recursion requires both δA and A at one of the frequencies [10]. (In the iterative method, the initial values of these quantities are only needed to begin the iteration; it is only in the constrained solutions where accurate values of δA and A are needed [14, 17].) Of course, there are other approaches, such as the Bayesian, for solving for the PSD parameters [21, 22]. Nevertheless, in most of these approaches, accurate constraints on the path attenuations are useful, particularly for moderate and heavy rainfall rates.

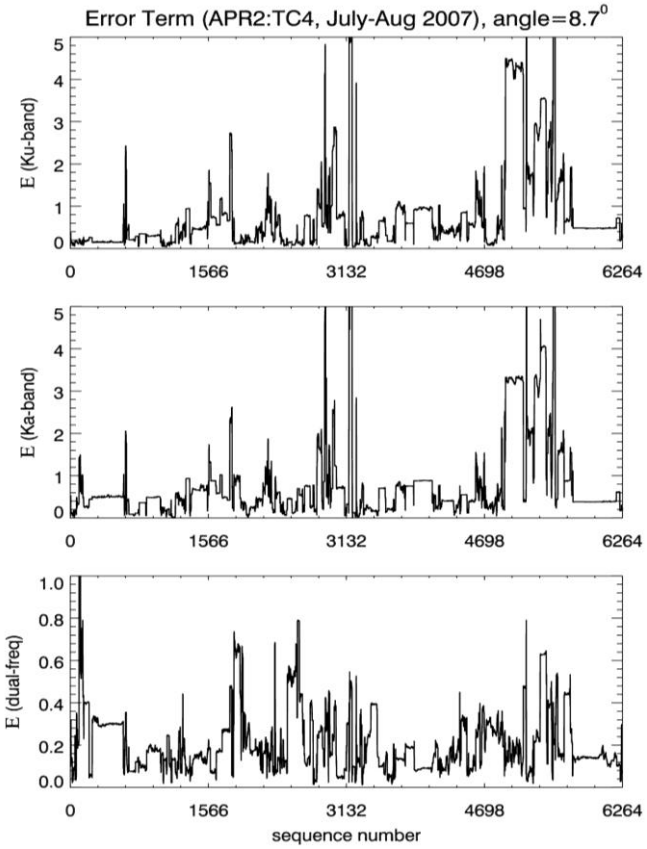

Fig. 7. The error term E for Ku-band (top), Ka-band (center) and differential (bottom).

To derive the path attenuation at Ka-band, say, from δA, one possible estimator is a simple multiplicative scaling:

$$\hat{A}'_{Ka} = \gamma \delta A \tag{11}$$

where the prime notation is used to distinguish an estimate derived from δA from an estimate derived directly from the SRT. If (11) is treated as a regression equation, then γ is given by:

$$\gamma = E(xy)/E(x^2)$$

where

$$y = \hat{A}'_{Ka} \approx \Delta h \sum_i k(f_1, PSD_i, T_i) \tag{12}$$

$$x = \delta A \approx \Delta h \sum_i [k(f_1, PSD_i, T_i) - k(f_2, PSD_i, T_i)]$$

where Δh denotes a fixed layer height, and PSD_i, T_i denote the particle size distribution and temperature of the ith layer. The quantity k represents the specific attenuation (dB/km) that can be computed from the PSD, temperature, and frequency. Using approximately 22,000 minutely-averaged raindrop size distributions, the computations have been done in a number of ways by taking different sets of temperatures and differing numbers of height levels. It is also straightforward to make the PSDs fully correlated between height levels (by taking the same PSD) or uncorrelated (by using a different PSD for each height level). Although there are some variations in the results depending on the nature of the assumed PSD correlation and temperature variations, the variations are generally small and $\gamma \approx 1.2$. (It should be noted, however, that the addition of various amounts of cloud water and mixed phase precipitation to the model could increase significantly the amount of variability in γ relative to the all-rain model used here.) We assume that the variance of δA can be approximated by E_{dual} with values given by Table 2 so that:

$$\mathrm{var}(\hat{A}'_{Ka})/E^2(\hat{A}'_{Ka}) = \gamma^2 \mathrm{E}^2_{dual}/\gamma^2 \delta A^2 = \mathrm{E}^2_{dual}/\delta A^2 \tag{13}$$

Similarly, using the definition of δA, (11) can be rearranged to yield

$$\hat{A}'_{Ku} = (\gamma - 1)\delta A \tag{14}$$

Then

$$\mathrm{var}(\hat{A}'_{Ku})/E^2(\hat{A}'_{Ku}) = (\gamma-1)^2 \mathrm{E}^2_{dual}/(\gamma-1)^2 \delta A^2 = \mathrm{E}^2_{dual}/\delta A^2 \tag{15}$$

Under the approximations used, the coefficients of variation for the two estimates are the same. It is useful to compare these results with the normalized variances of A_{Ka} and A_{Ku} derived directly from the Ka-band and Ku-band surface data. To the same level of approximation as above:

$$\mathrm{var}(\hat{A}_{Ka})/E^2(\hat{A}_{Ka}) \approx (\mathrm{E}_{Ka}/\gamma\delta A)^2 \approx 0.7 \times (\mathrm{E}_{Ka}/\delta A)^2 \tag{16}$$

$$\mathrm{var}(\hat{A}_{Ku})/E^2(\hat{A}_{Ku}) \approx (\mathrm{E}_{Ku}/(\gamma-1)\delta A)^2 \approx 25 \times (\mathrm{E}_{Ku}/\delta A)^2 \tag{17}$$

where E_{Ku} and E_{Ka} are the standard deviations associated with the single-frequency SRT as shown in Table 2. Comparisons of the normalized variances of the Ka-band estimates given by (13) and (16) show that the better estimate is determined by the relative magnitudes of $\sqrt{0.7}\ E_{Ka}$ and E_{dual}; values from Table 2 indicate that the later quantity is smaller than the former for most incidence angles and where the improvement increases with increasing incidence angle. Comparisons of the A_{Ku} normalized variances given by (15) and (17) show that the better estimate is determined by the relative magnitudes of $5\ E_{Ka}$ and E_{dual}, indicating that estimates of A_{Ku} derived from the differential attenuation should constitute a significant improvement in accuracy over the single-frequency SRT result.

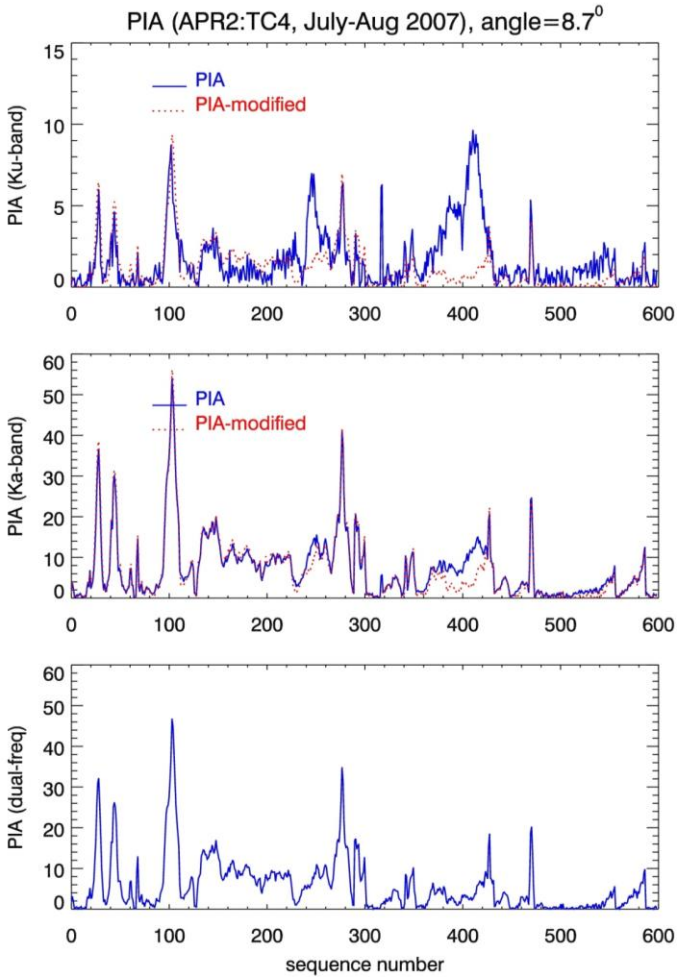

Fig. 8. A portion of data showing comparisons of the directly retrieved PIA (blue) with that derived from the differential PIA (red). Top panel: Ku-band; Center panel: Ka-band. For reference, the differential attenuation is shown in the bottom panel.

It is instructive to look at results from measured data. Comparisons of A_{Ku} and A'_{Ku} are shown in the upper panel while comparisons of A_{Ka} and A'_{Ka} are shown in the middle panel of Fig. 8. Note that in the figure, the 'modified PIA' is that derived from δA while the 'PIA' is derived from the single-frequency SRT. Comparisons between A_{Ka} and A'_{Ka} at this and other angles generally show good correlations. On the other hand, comparisons between A_{Ku} and A'_{Ku} indicate a large amount of scatter. This is exhibited more clearly in Fig. 9 which shows scatter plots of A_{Ku} versus A'_{Ku} in the top panel and A_{Ka} versus A'_{Ka} results in the bottom panel. It is assumed that the much larger scatter in the top scatter plot is the result of the high error variance associated with the single-frequency SRT method at Ku-band.

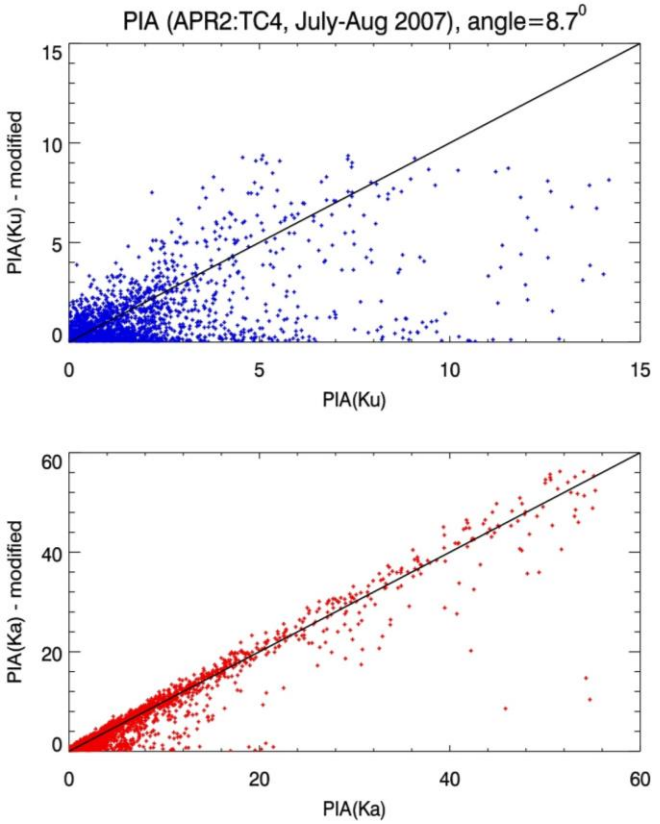

Fig. 9. Scatter plots of PIA estimates derived from the single-frequency SRT (abscissa) versus the PIA derived from the differential estimate (ordinate). Top: Ku-band; Bottom: Ka-band.

V. SUMMARY

A simple analysis of a dual-frequency surface reference technique shows that the variance of the estimate depends on the variance of the surface cross sections and their correlation. In analyzing the problem using the JPL APR 2 airborne radar data, a measure of the error in the path attenuation estimates was taken to be a weighted rms error among the various reference data sets that can be formed to estimate this quantity. This was used to obtain a preliminary assessment of the behavior of the dual-frequency SRT relative to its single-frequency counterpart. Since both the differential path and single-frequency attenuations are needed in solving the equations for parameters of the PSD, a simple estimator of A_{Ka}

from δA was proposed. Preliminary results indicate that both δA and the derived A_{Ka} quantities should prove useful in improving the constraints used in dual-wavelength radar retrievals of precipitation parameters from airborne and spaceborne platforms.

ACKNOWLEDGMENT

We wish to thank Rafael Rincon of NASA/GSFC for providing the measured drop size distributions and Jeffrey Jones of Wyle Information Systems for advice in processing the data. A portion of this research (Tanelli and Durden) was carried out at the Jet Propulsion Laboratory, California Institute of Technology, under a contract with the National Aeronautics and Space Administration. This work is supported by Dr. R. Kakar of NASA Headquarters under NASA's Precipitation Measurement Mission Grant NNH06ZDA001N-PMM.

REFERENCES

[1] R. Meneghini, J. Eckerman, and D. Atlas, "Determination of rain rate from a spaceborne radar using measurements of total attenuation," *IEEE Trans. Geosci. Remote Sens*., vol. **21**, pp. 34-43, 1983.

[2] L. Li, E. Im, L.N. Connor, and P.S. Chang, "Retrieving ocean surface wind speed from the TRMM precipitation radar measurements," *IEEE Trans. Geosci. Remote Sens.*, vol. **42**, pp. 1271-1282, 2004.

[3] S. L. Durden, L. Li, E. Im and S.H. Yueh, "A surface reference technique for airborne Doppler radar measurements in hurricanes," *J. Atmos. Oceanic Technol.*, vol. **20**, pp. 269-275, 2003.

[4] S. L. Durden and Z. S. Haddad, "Comparison of radar rainfall retrieval algorithms in convective rain during TOGA COARE," *J. Atmos. Oceanic Technol*., vol. **15**, pp. 1091-1096, 1998.

[5] L. Li, E. Im, S.L. Durden, and Z. S. Haddad, "A surface wind model-based method to estimate rain- induced radar path attenuation over ocean," *J. Atmos. Oceanic Technol*, vol. **19**, pp. 658-672, 2002.

[6] R. Meneghini, J.A. Jones, T. Iguchi, K. Okamoto, and J. Kwiatkowski, "A hybrid surface reference technique and its application to the TRMM Precipitation Radar," *J. Atmos. Oceanic Technol*., vol. **21**, pp. 1645-1658, 2004.

[7] S. Seto and T. Iguchi, "Rainfall-induced changes in actual surface backscattering cross sections and effects on rain-rate estimates by spaceborne Precipitation Radar," *J. Atmos. Oceanic Technol.*, vol. **24**, pp. 1693-1709, 2007.

[8] T. Iguchi, T. Kozu, J. Kwiatkowski, R. Meneghini, J. Awaka, and K. Okamoto, "Uncertainties in the rain profiling algorithm for the TRMM Precipitation Radar," *J. Meteor. Soc. Japan*, vol. **87A**, pp. 1-30, 2009.

[9] S. Tanelli, S.L. Durden, and E. Im, "Simultaneous measurements of Ku- and Ka-band sea surface cross sections by an airborne radar," *IEEE Geosc. Remote Sens. Letters*, vol. **3**, pp. 359-363, 2006.

[10] R. Meneghini, and J.A. Jones, "Standard deviation of spatially-averaged surface cross section data from the TRMM Precipitation Radar," *IEEE Geosc. Remote Sens. Letter*s, vol. **8**, pp. 293-297, 2011.

[11] R. Meneghini, J.A. Jones, and L.H. Gesell, "Analysis of a dual-wavelength surface reference radar technique," *IEEE Trans. Geosci. Remote Sens*., vol. **GE25**, pp. 456-471, 1987.

[12] R. Meneghini, H. Kumagai, J.R. Wang, T. Iguchi, and T. Kozu, "Microphysical retrievals over stratiform rain using measurements from an airborne dual-wavelength radar-radiometer," *IEEE Trans. Geosci Remote Sens*., vol. **35**, pp. 487-505, 1997.

[13] L. Liao and R. Meneghini,"A study of air/space-borne dual-wavelength radar for estimation of rain profiles. *Advances in Atmos. Sci*., vol. **22**, pp. 841-851, 2005.

[14] R. Mardiana, T. Iguchi and N. Takahashi, "A dual-frequency rain profiling method without the use of a surface reference technique," *IEEE Trans. Geosci. Remote Sens.*, vol. **42**, 2214-2225, 2004.

[15] C.R. Rose and V. Chandrasekar, "A GPM dual-frequency retrieval algorithm: DSD profile-optimization method. *J. Atmos. Oceanic Technol.*, vol. **23**, pp. 1372-1383, 2006.

[16] L. Liao, R. Meneghini, L. Tian, and G.M. Heymsfield, "Measurements and simulations of nadir-viewing radar returns from the melting layer at X and W bands," *J. Appl. Meteor Climatol*., vol. **48**, pp. 2215-2226, 2009.

[17] S. Seto and T. Iguchi, "Applicability of the iterative backward retrieval method for the GPM dual-frequency precipitation radar," *IEEE Trans. Geosci. Remote Sens*., 2011 (in press).

[18] S.L. Durden, Z.S. Haddad, A. Kitiyakara, and F.K. Li, "Effects of nonuniform beam filling on rainfall retrieval for the TRMM Precipitation Radar," *J. Atmos. Oceanic Technol*., vol. **15**, pp. 635-646, 1998.

[19] T. Kozu and T. Iguchi, "Nonuniform beamfilling correction for spaceborne radar rainfall measurement: Implications from TOGA COARE Radar data analysis," *J. Atmos. Oceanic Technol*., vol. **16**, pp. 1722-1735, 1999.

[20] G.A. Sadowy, A.C. Berkun, W. Chun, E. Im, and S.L. Durden, "Development of an advanced airborne precipitation radar," *Microwave J*., vol. **46**, pp. 84-98, 2003.

[21] M. Grecu, L. Tian, W.S. Olson, and S. Tanelli, "A robust dual-frequency radar profiling algorithm," *J. Appl. Meteor Climatol.* (submitted).

[22] Z. S. Haddad, J. P. Meagher, S. L. Durden, E. A. Smith, and E. Im, "Drop Size Ambiguities in the Retrieval of Precipitation Profiles from Dual-Frequency Radar Measurements," *J. Atmos. Sci*., vol. **63**, pp. 204–217, 2006.

Table 1. Statistics (in dB) of NRCS over Ocean as a function of Incidence Angle (from Nadir)

Angle (deg)	$<\sigma^0(Ku)>$	$<\sigma^0(Ka)>$	Std[σ^0(Ku)]	Std[σ^0(Ka)]	ρ
2.2	12	10.4	1.5	1.5	0.58
4.4	10.9	9.1	1.1	1.3	0.73
6.5	9.0	7.4	1.5	1.4	0.86
8.7	6.4	4.9	2.4	2.3	0.95
10.9	3.5	2.1	3.3	3.4	0.98
13	0.56	-0.9	4.2	4.7	0.98
15.2	-2.4	-4	4.9	5.9	0.99
17.4	-5.4	-7	5.5	6.8	0.99
19.6	-8.3	-9.8	5.9	7.4	0.99
21.7	-10	-11.4	5.7	7.2	0.99

Table 2. Error term (in dB) versus incidence angle for Ku, Ka and dual-frequencies

Incidence Angle (deg)	$<E>_{Ku}$	$<E>_{Ka}$	$<E>_{dual}$
2.2	0.45	0.51	0.34
4.4	0.38	0.39	0.26
6.5	0.52	0.50	0.24
8.7	0.67	0.66	0.20
10.9	0.84	0.87	0.20
13	1.02	1.07	0.26
15.2	1.26	1.44	0.32
17.4	1.39	1.7	0.41
19.6	1.65	2.1	0.44
21.7	1.87	2.35	0.48